Available online at www.sciencedirect.com
SCIENCE DIRECT
Polymer 46 (2005) 5118–5124
polymer
www.elsevier.com/locate/polymer

Thin crystal melting produces the low-temperature endotherm in ethylene/methacrylic acid ionomers

Yueh-Lin Loo[a,1], Katsuyuki Wakabayashi[a], Y. Evelyn Huang[a,2], Richard A. Register[a,*], Benjamin S. Hsiao[b]

[a]*Department of Chemical Engineering, Princeton University, Princeton, NJ 08544, USA*
[b]*Department of Chemistry, State University of New York at Stony Brook, Stony Brook, NY 11794, USA*

Received 8 February 2005; received in revised form 20 April 2005; accepted 20 April 2005
Available online 11 May 2005

Abstract

Upon extended aging at room temperature, ethylene/methacrylic acid (E/MAA) ionomers develop an endotherm near 50 °C in their differential scanning calorimetry traces. The origin of this low-temperature endotherm has been the subject of considerable debate, in part because direct structural probes have been little applied to its study. Here, we use in situ small-angle X-ray scattering and wide-angle X-ray diffraction to show that this endotherm reflects the melting of thin polyethylene crystals, which gradually develop following primary crystallization. These secondary crystals form within the amorphous layers separating primary crystals. When the framework of primary crystals is oriented by crystallization during flow, the secondary crystals follow this orientation, indicating that the secondary crystals are not isometric fringed micelles but instead have a substantial lateral extent.

Keywords: Ionomer; Secondary crystals; Small-angle X-ray scattering

1. Introduction

Ionomers are organic polymers, where a small fraction (usually less than 10%) of the repeat units bear pendant ionic groups, such as carboxylate salts [1]. In bulk, electrostatic forces cause the ionic groups to associate, producing nanometer-size ion-rich aggregates dispersed in a polymer matrix largely depleted of ions. Crystallizable ionomers, such as the salts of ethylene/methacrylic acid statistical copolymers, E/MAA, have a more complex morphology comprising polyethylene (PE) crystals, amorphous polymer chain segments, and ionic aggregates [2,3]. This structural complexity can produce correspondingly complex thermal and thermomechanical behavior in these materials.

One feature which has attracted considerable attention in E/MAA ionomers is a low-temperature endotherm in the differential scanning calorimetry (DSC) trace, an endotherm that develops during room-temperature annealing (storage) over a period of days to months [4]. The solid curve in Fig. 1 represents the DSC trace for a typical aged E/MAA ionomer. Typical peak temperatures for this endotherm (T_2) are $\approx$50 °C (43 °C in Fig. 1), well below the melting temperature (T_m) of the primary PE crystallites near 95 °C. Annealing at temperatures moderately above room temperature (but still well below T_m) increases T_2 [5,6]. Dynamic mechanical thermal analysis shows a significant drop in the storage modulus (E') when T_2 is crossed [7]. Fig. 1 also shows the reversing and non-reversing components of the heat flow, as obtained from dynamic (modulated) DSC [8]. The low-temperature endotherm appears in the non-reversing component of the heat flow, indicating that there is an energetic barrier to forming the structures responsible [9]—consistent with the endotherm's slow development upon room-temperature storage. We have examined a range of E/MAA ionomers, neutralized

* Corresponding author. Tel.: +1 609 258 4691; fax: +1 609 258 0211.
E-mail address: register@princeton.edu (R.A. Register).
[1] Present address: Department of Chemical Engineering, The University of Texas at Austin, Austin, TX 78712, USA.
[2] Present address: Bloomberg L.P., 731 Lexington Ave., New York, NY 10022, USA.

0032-3861/$ - see front matter © 2005 Elsevier Ltd. All rights reserved.
doi:10.1016/j.polymer.2005.04.043

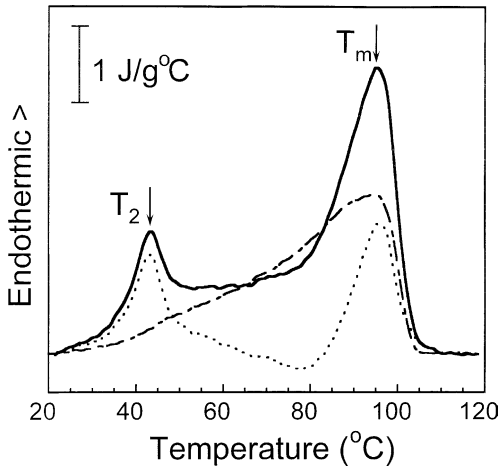

Fig. 1. Dynamic differential scanning calorimetry (DDSC) traces for a typical E/MAA ionomer (11.5 wt% MAA, neutralized 16% with Na^+, stored 6 months at room temperature). (—) total heat flow, equivalent to conventional DSC trace; (- · -) reversing heat flow; (· · ·) non-reversing heat flow. For ease of comparison, all traces have had a linear baseline (tangent to high- and low-temperature ends of scan) subtracted. Peak temperatures for primary crystal melting (T_m) and the low-temperature endotherm (T_2) are indicated.

with different cations and to different levels, and the dynamic DSC (DDSC) results for all materials show the same qualitative features which Fig. 1 exhibits [6].

The original explanation for this feature, proposed by Marx and Cooper [4], is that it reflects the melting of small 'secondary' PE crystallites, which slowly form following primary crystallization. Several subsequent papers have interpreted their results following this model [5,7,10]. Similar low-temperature endotherms have subsequently been seen in other compositionally homogeneous ethylene copolymers, such as those synthesized from metallocene catalysts, and were also attributed to the melting of thin secondary crystals [11]. However, several other publications have attributed the low-temperature endotherm in E/MAA ionomers to an order–disorder transition within the ionic aggregates [12–15]. This explanation is distinct from a possible dissociation of the ionic aggregates; in E/MAA ionomers, the aggregates are known to persist up to the ionomer's decomposition temperature (>300 °C) [16].

To date, this transition has been investigated largely by indirect (calorimetric [4–7,12–14] mechanical [7,12,14], and spectroscopic [10,15,17]) probes of structure, so these two conflicting interpretations have persisted in the literature. Surprisingly, variable-temperature X-ray scattering—a probe capable of definitively testing the secondary crystal hypothesis—has not yet been applied to this problem. Here, we use a combination of X-ray scattering techniques (small and wide-angle, one- and two-dimensional) to show that the low-temperature endotherm does indeed result from the melting of secondary crystals. Moreover, we demonstrate that these crystals are interlamellar, forming between the primary crystals, and that their habit is generally more akin to that of a lamellar crystallite than an isometric fringed micelle.

2. Experimental

Two different zinc-neutralized E/MAA ionomers, and one sodium-neutralized ionomer, were employed in this work. E/MAA copolymers, such as those from which these ionomers were derived, are produced by a high-pressure free radical polymerization similar to that used for the production of low-density polyethylene (LDPE). This process yields little chemical heterogeneity between chains [18], though the copolymers are highly polydisperse and contain both long-chain and short-chain branches. The first zinc ionomer, Zn80-11, was based on a copolymer [19,20] containing 11.5 wt% MAA (4.1 mol% MAA), with a copolymer melt index [21] of 100 g/10 min (ASTM D1238 condition E), and a weight-average molecular weight of 71 kg/mol; 80% of the MAA residues were neutralized with Zn^{2+} to generate the ionomer, which was provided by DuPont. Pellets of Zn80-11 were melt-pressed into an isotropic, ≈1 mm thick sheet at 150 °C, and the sheet allowed to slow-cool to room temperature at ≈1 °C/min. The sheet was stored at room temperature for 17 days prior to the X-ray scattering measurements.

The sodium ionomer, Na16-11, was based on the same E/MAA copolymer as Zn80-11, but had 16% of the MAA residues neutralized with Na^+ in a solution process described elsewhere [19]. A 5.13 mg specimen of Na16 was encapsulated in a DSC pan, heated to 120 °C to fully melt the specimen and ensure good thermal contact with the pan, quenched to room temperature at 50 °C/min, removed from the DSC, and stored at room temperature for 6 months prior to conducting the dynamic DSC (DDSC) measurements presented in Fig. 1.

The second zinc ionomer, Zn46-12, was based on a copolymer containing 12 wt% MAA (4.3 mol% MAA), with a copolymer melt index of 13.5 g/10 min; 46% of the MAA residues were neutralized with Zn^{2+} at DuPont to generate the ionomer. Zn46-12 was blown into 2-mil (50 μm thick) film on a laboratory-scale blowing line, as described elsewhere [22]. The particular specimen employed here was processed with a blowup ratio of 1.5, die temperature of 218 °C, and a frost line height of 10 cm, which generates a highly anisotropic film with the primary PE crystallites stacked along the machine direction [22]. The sample was stored at room temperature for 37 months prior to the measurements described herein.

To probe the structural changes which occur upon heating Zn80-11 through the low-temperature endotherm, we employed time-resolved simultaneous small-angle X-ray scattering (SAXS) and wide-angle X-ray diffraction (WAXD) at the Advanced Polymer Beamline (X27C) at the National Synchrotron Light Source, Brookhaven National Laboratory. The incident beam was collimated

by a three-pinhole assembly. Two one-dimensional gas-filled wire detectors were used for data collection. The magnitude of the momentum transfer vector q is defined as $q \equiv (4\pi/\lambda)\sin\theta$, where λ is the X-ray wavelength (0.1307 nm, which has an energy below the Zn absorption edge to limit fluorescence) and 2θ is the scattering angle. A Linkam DSC600 was used for precise temperature control during the heating ramp. Samples were loaded at 4 °C and were ramped from the loading temperature into the melt at 10 °C/min. The time resolution of the measurements was 6 s. For calculating integrated metrics (relative invariant, integrated WAXD intensity), the individual 6-s frames were of sufficient statistical quality, but when presenting SAXS profiles or extracting parameters related to their shape (e.g. peak position), five sequential frames were binned together and the temperature assigned as the midpoint of the set.

Two-dimensional SAXS measurements on the anisotropic Zn46-12 blown film were conducted using a laboratory X-ray system comprising a Cu K_α X-ray source, a Statton (pinhole) camera, and Kodak image plates read with a Molecular Dynamics PhosphorImager SI, providing a digital diffraction pattern directly [22,23]. Blown film samples were cut and stacked to a thickness of 1.5 mm with great care to match the orientation through the stack. Measurements at elevated temperature employed the original Statton camera hotstage (W. H. Warhus, Inc.), retrofitted with a digital temperature controller to provide stability within ± 1 °C. SAXS patterns were acquired upon heating in 5 °C increments from 45 to 75 °C, with 45 min required for data collection and 15 min to step between temperatures, for an average heating rate of 5 °C/h.

Both conventional DSC and DDSC measurements were conducted on a Perkin–Elmer DSC-7 equipped with an intracooler, calibrated with indium and tin or mercury, and running Pyris software. For conventional DSC scans, a heating ramp of 10 °C/min was used, starting at 20 °C. For DDSC, the temperature profile consisted of alternating 30-s heating ramps (at 2 °C/min) and 30-s isothermal holds, for an effective heating rate of 1 °C/min; the scans extended from 20 to 120 °C. Home-written software [6] based on published equations [8] was used to extract the total, reversing, and non-reversing heat capacities.

3. Results and discussion

3.1. One-dimensional SAXS/WAXD

SAXS and WAXD patterns were collected simultaneously as Zn80-11 was heated from 4 °C into the melt. Fig. 2 contains representative SAXS profiles taken at several points during the heating scan. In this angular region, only scattering from the crystallites is visible; the 'ionomer peak', due to scattering from the ionic aggregates within the amorphous regions, is relatively weak and at significantly higher $q(\approx 2\ \mathrm{nm}^{-1})$ [24], outside the range of

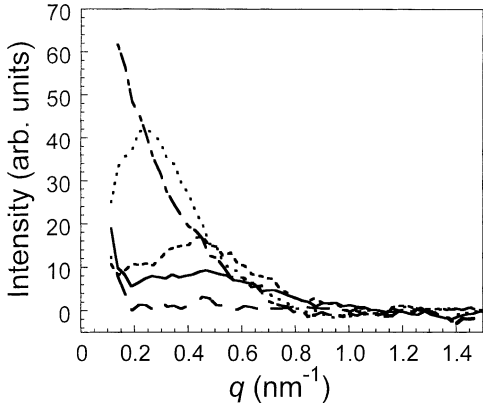

Fig. 2. SAXS profiles for Zn80-11 taken during the 10 °C/min heating ramp, at (—) 6, (- - -) 47, (· · ·) 74, (- · -) 85, and (– –) 111 °C.

our SAXS measurements. The peak moves to lower q and grows substantially in intensity with increasing temperature, until the primary PE crystal T_m is reached. Fig. 3 shows how the Bragg spacing d of this reflection changes with temperature:

$$d = 2\pi/q^* \tag{1}$$

where q^* is the position of the peak in a plot of $q^2 I$ vs. q, and I is the SAXS intensity; the q^2 factor is an appropriate first-order correction for the form factor of plate-like objects [25], such as lamellar crystals. However, the same general trends are evident when q^* is extracted from a plot [26] of I vs. q. Below 40 °C, d remains approximately constant (average 10.0 nm, standard deviation 0.5 nm), while above 45 °C, d increases rapidly with temperature. Room-temperature aging provides scant undercooling to form crystals with melting points below 40 °C, and the specimen was cooled only briefly to 4 °C on loading into the hot stage, so the observation of a near-constant d from 4 to 40 °C is not surprising. The DSC trace for Zn80-11 is shown in the top portion of Fig. 4; the low-temperature endotherm appears to start near 40 °C, coincident with the end of the constant-d region. In Zn80-11 crystallized by slow cooling, this

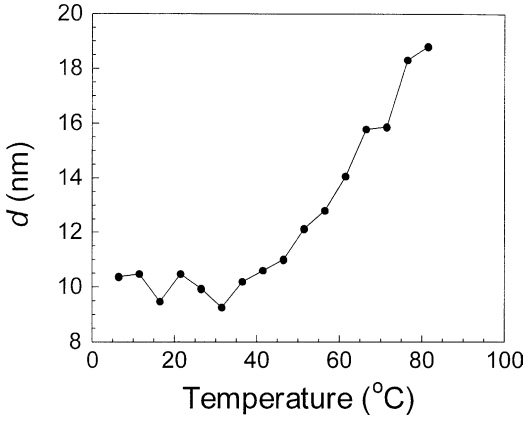

Fig. 3. SAXS Bragg spacing d for Zn80-11 during the 10 °C/min heating ramp.

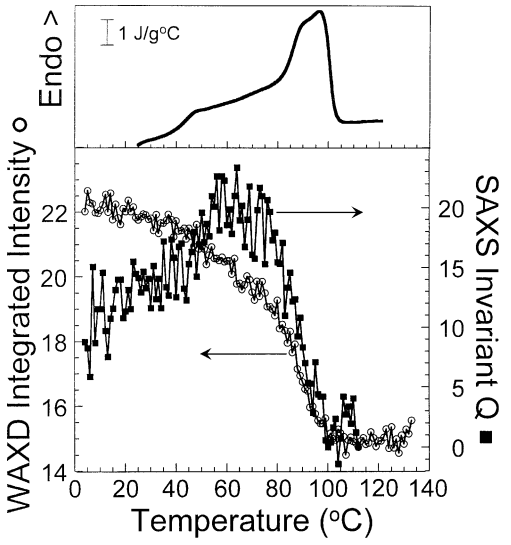

Fig. 4. Top panel: DSC heating thermogram of Zn80-11 at 10 °C/min. Bottom panel: integrated intensity of the PE (110) WAXD reflection (○, left axis) and relative SAXS invariant Q (■, right axis) for Zn80-11 during the 10 °C/min heating ramp.

low-temperature endotherm is relatively modest and extends over a broad temperature range, up to ≈80 °C where the primary endotherm begins to emerge. From the integrated area of the DSC trace, and the enthalpy of fusion of fully crystalline polyethylene [27] (279 J/g), we estimate Zn80-11 to be 39 wt% crystalline at room temperature.

The Bragg spacing d is commonly identified as the average repeat distance of crystals throughout the stack [28], in analogy with Bragg diffraction from a perfect crystal; as the lower-melting crystals are removed from the stack, one would thus expect d to increase, as observed. However, the lamellar stacks in crystalline polymers are far from perfect, so this interpretation is open to question. Recently, Crist [29] has shown that for relatively narrow distributions of crystalline and amorphous layer thicknesses, the melting of individual crystals within a stack leads to no significant change in the Bragg spacing prior to the last stages of melting. With such narrow thickness distributions, the amorphous layers which result from the melting of individual crystals are so much thicker than the original amorphous layers that their distributions do not overlap; consequently, while the average intercrystal spacing is increased by the melting of isolated crystals, the most probable spacing remains at its original location, and the position of the SAXS peak does not change. However, when the amorphous layer thickness distributions are broad and flat, this situation does not pertain, and the SAXS peak shifts as a consequence of such melting, as evidenced in the SAXS patterns calculated for simulated lamellar stacks [30].

The lower part of Fig. 4 shows the integrated intensity of the PE (110) WAXD reflection during the heating ramp. Below 40 °C, the (110) intensity changes weakly and linearly with temperature. No substantial structural changes are occurring in this temperature range; the small change in WAXD intensity (approximately 0.08%/°C) can be attributed to the material's thermal expansion, leading to a smaller mass within the irradiated volume, plus increasing thermal disorder within the crystals. Above 40 °C, the (110) intensity decreases at an accelerating rate, but the change is modest until the primary PE crystals begin to melt near 80 °C. Yet between 40 and 60 °C, Fig. 3 shows that there is a 35–40% increase in d, indicating a corresponding increase in the average spacing between the crystallites. In statistical copolymers such as these, the primary crystals are incapable of substantial thickening; their thickness distribution reflects the crystallizable sequence length distribution, coupled with kinetic constraints [31]. Consequently, the increase in d must reflect the selective melting of crystals, such that the remaining crystals have a greater average spacing.

Thus, the picture in Fig. 5 emerges, where the low-temperature endotherm reflects the melting of thin crystals which form between the primary crystals during slow cooling or room-temperature storage. Some ethylene sequences which are long enough to crystallize may fail to do so during primary crystallization; on slow-cooling or aging, these uncrystallized segments can form smaller secondary crystals between the existing primary crystals. Such secondary crystallization is not unusual for random copolymers [11], as noted originally by Marx and Cooper [4], though this low-temperature endotherm is typically much more pronounced for ionomers than for E/MAA copolymers or low-density polyethylene (LDPE). In ionomers, aggregation of the ionic groups produces a high local viscosity [19,20] which impedes the diffusion of crystallizable segments. This is also evident in the slower rate of primary crystallization as compared with unneutralized E/MAA copolymers [5]. Consequently, in E/MAA ionomers, more crystallizable segments remain amorphous at the completion of primary crystallization, which in turn generate the larger low-temperature endotherm upon extended room-temperature aging.

Since our measurements do not directly probe the ionic

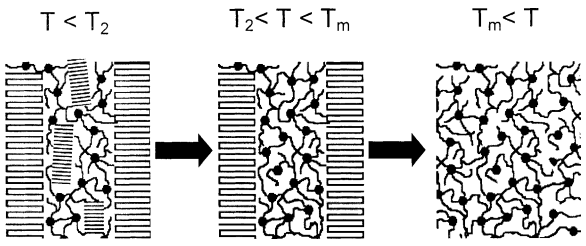

Fig. 5. Schematic of the structural changes which occur in E/MAA ionomers on heating. Straight segments indicate PE crystal stems; circles represent ionic aggregates. Left to center: the thinner secondary PE crystals (located between primary PE crystals) melt when the sample is heated through the low-temperature endotherm at T_2. Center to right: further heating through the primary crystal T_m results in an amorphous, molten polymer matrix with ionic aggregates distributed uniformly throughout. Primary crystals are drawn with regular chain folding while secondary crystals are represented as bundle-like; this is schematic only, as the actual structure of the crystal surfaces is unknown.

aggregates, they cannot preclude the possibility that an order–disorder transition within the ionic aggregates [12–15] could be occurring simultaneously with the melting of these secondary crystals. However, extended X-ray absorption fine structure (EXAFS) measurements by Farrell and Grady [32] on a 57% Zn^{2+} neutralized ionomer, prepared from the same E/MAA copolymer as Zn80-11, revealed no significant changes in the aggregates' internal order upon heating through T_2, bearing against this interpretation. Moreover, our results clearly show that such an ionic order-disorder transition need not be postulated: a significant population of secondary crystals is certainly present in these E/MAA ionomers, and their melting is sufficient to explain the observed low-temperature endotherm.

As a rough approximation, if we take the values of the interfacial energy (0.0874 J/m^2) and enthalpy of fusion for linear polyethylene [27] and apply them to Zn80-11, the Gibbs–Thomson equation [27] indicates that the primary crystals (with $T_m = 95$ °C) have a thickness of approximately 6 nm, while the secondary crystals (with $T_2 = 50$ °C) have a thickness of approximately 3 nm. Taking as a simple model a bidisperse crystal thickness distribution, with thick and thin crystals stacked in random sequence, a 25:75 number ratio of thin:thick crystals would produce the observed change in d between 40 and 60 °C, yet the thin crystals would constitute only 14% of the mass of the crystalline phase, consistent with the modest area of the low-temperature endotherm revealed by DSC in Fig. 4, and with the modest decrease in WAXD (110) intensity. SAXS is clearly the most sensitive technique for detecting the presence of these thin crystals.

In addition to the change in SAXS peak position, the SAXS intensity also changes in an unusual way during the heating ramp, as exemplified by the profiles in Fig. 2. The integrated SAXS intensity carries information on the heterogeneity in the system: phase volume fractions and electron density contrasts. In the angular range of interest here ($q < 1$ nm^{-1}), this complex E/MAA ionomer can be approximated as containing two phases: a crystalline PE phase (both primary and secondary crystals) and an amorphous phase containing both uncrystallized polymer chain segments and ionic aggregates [3]. Hence, by integrating q^2I over the small-q range ($0.12 < q < 0.8$ nm^{-1}), we obtain a 'relative invariant' (Q) by which morphological changes on the length scale of the crystallites can be gauged. Q is related to the system's heterogeneity as [33]:

$$Q \sim \phi_c(1 - \phi_c)(\Delta\rho)^2 \tag{2}$$

where ϕ_c is the volume fraction of crystallites and $\Delta\rho$ is the electron density difference between the PE crystallites (ρ_c) and the amorphous phase (ρ_a). The bottom portion of Fig. 4 shows that Q increases slowly on heating from 10 to 45 °C, then increases steeply between 45 and 60 °C, then decreases above 70 °C. From 10 to 45 °C, the system is essentially static; Q increases because the amorphous phase has a higher thermal expansion coefficient than the crystalline phase, and $\rho_c > \rho_a$, so $\Delta\rho$ increases with temperature. Such a slow but steady increase in Q with temperature is commonly observed in crystalline polymers well below the melting point, including polyethylene [34]. If representative values for the thermal expansion coefficient are assumed for the crystalline and amorphous phases (3 and 7×10^{-4} °C^{-1}, respectively), then the observed increase in Q from 10 to 45 °C (0.9%/°C) translates to a room-temperature electron density contrast of 23 nm^{-3} for Zn80-11, vs. 50 nm^{-3} for polyethylene. Indeed, at room temperature (below T_2), the SAXS pattern of Zn80-11 has a significantly weaker integrated intensity (relative invariant) than does its parent E/MAA copolymer or a comparable low-density polyethylene (by $\approx 6\times$ vs. the latter) [35]. The electron density contrast of 23 nm^{-3} translates to an amorphous-phase mass density of 0.978 g/cm^3, and an effective mass density of the partially Zn-neutralized methacrylate units of 1.85 g/cm^3, assuming pure polyethylene crystals and additivity of component specific volumes.

Above 70 °C, the primary crystals begin to melt, and since $\phi_c < 1/2$, a reduction in ϕ_c leads to a decrease in Q, following Eq. (1). The most interesting observation is the steep increase in Q between 45 and 60 °C, corresponding to the low-temperature endotherm. Melting the secondary crystals will reduce ϕ_c, which by itself should produce a modest decrease in Q (by $\approx 6\%$, if the secondary crystals are $\approx 14\%$ of the mass of the crystalline phase). But melting the secondary crystals also influences ρ_a, which is a weighted average over amorphous PE segments ($\rho_{a,E}$) and the methacrylic acid and ionic groups (ρ_{ion}), where $\rho_{ion} > \rho_{a,E}$. When the secondary crystals melt, the acid and ionic groups in the amorphous phase are diluted with additional amorphous ethylene segments, reducing ρ_a and increasing $\Delta\rho$. Using the same effective mass density of 1.85 g/cm^3 at room temperature for the partially-neutralized methacrylate units, an increase of 20% in Q is calculated upon melting the secondary crystals (considering both the decrease in ϕ_c and the increase in $\Delta\rho$, the latter again assuming additivity of component specific volumes), which compares very favorably with the 20% increase in Q observed in Fig. 2 between 45 and 60 °C, above the straight-line extrapolation of Q from 10 to 45 °C.

3.2. Two-dimensional SAXS

Crystallization during flow, such as during injection molding or film blowing, can strongly orient the primary crystals. But the secondary crystals form quiescently, upon storage, so the secondary crystals must form with an orientation consistent with the constraints imposed by the pre-existing framework of primary crystals. For example, if primary crystallization leaves relatively large (micron-scale) pockets of amorphous material (e.g. interspherulitic or interfibrillar), then the secondary crystals, which form within such pockets, would be essentially isotropic. By

contrast, if the primary crystals define a volume-filling framework and the secondary crystals form by insertion into this lamellar structure, then they must necessarily follow the general orientation of the primary crystals, as illustrated in the left panel of Fig. 5. Significant differences in orientation are possible only when the lateral extent of the secondary crystals is quite short, as in the classic 'fringed micelle' picture [36].

The 2D SAXS pattern from the Zn46-12 blown film is shown as the inset in Fig. 6. The 'two point' SAXS pattern indicates that the stacking direction for the lamellae lies predominantly along the meridian. Fig. 6 also shows one-dimensional 'cuts' of the 2D pattern at different temperatures, along the meridian (top panel) and equator (bottom panel), each averaged over $\pm 7.5°$ in azimuthal angle and multiplied by q^2. Two features are immediately apparent from the data. First, both the meridional and the equatorial traces show the same movement of the peak to lower q with increasing temperature found by synchrotron SAXS for Zn80-11. However, the effective heating rate in the laboratory 2D SAXS measurement is much slower, approximately 5 °C/h, which can permit rearrangement of the secondary crystals during the measurement prior to their final melting. Second, at any given temperature, the peak position (q^*) is slightly but systematically higher along the equator than along the meridian. This indicates that the relatively few crystals whose normals point along the equator (the transverse direction in the blown film) have a slightly smaller average intercrystal separation.

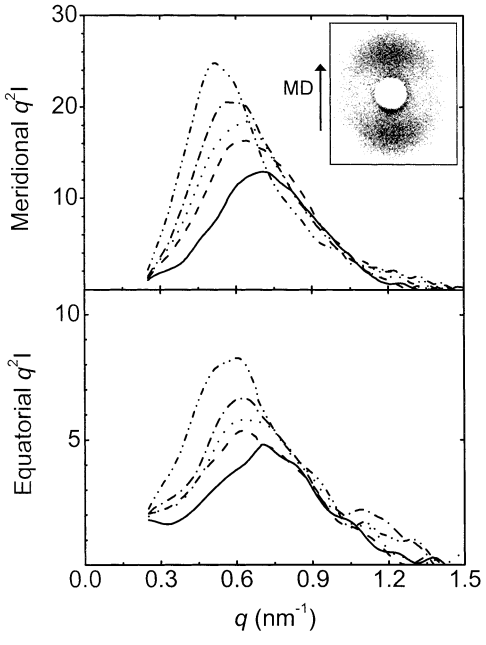

Fig. 6. Inset, top right: 2D SAXS pattern for the blown film of Zn46-12 at room temperature. The machine direction (MD) during film blowing is aligned with the meridian. Lorentz-corrected intensity q^2I along the meridian (top panel) and equator (bottom panel) at: (—) room temperature, (- - -) 45, (· · ·) 60, (- · -) 65, and (- · · -) 75 °C. All intensities have had a q-independent background subtracted prior to multiplication through by q^2, to remove scattering from thermal density fluctuations.

A relative invariant may again be computed by integrating q^2I over the range of interest ($0.25 \leq q \leq 1.2$ nm^{-1} here). The ratio of this quantity along the meridian vs. the equator (Q_{mer}/Q_{eq}) reflects the relative populations of crystals scattering in the two directions; this ratio is plotted in Fig. 7 as a function of temperature. The top portion of Fig. 7 also shows the DSC trace for the Zn46-12 blown film; compared with Zn80-11, the low-temperature endotherm is quite pronounced, since the blown film was rapidly crystallized and then aged at room temperature for over 3 years. If the scattering along the equator were due to isotropic secondary crystals, then heating above T_2 should drive Q_{eq} towards zero and produce a strong increase in the Q_{mer}/Q_{eq} ratio. Instead, very little change in Q_{mer}/Q_{eq} is seen between 25 and 75 °C, indicating that the secondary crystals also scatter predominantly along the meridian, as expected if they form by interlamellar insertion and are generally parallel to the primary crystals.

Though this observation indicates that the secondary crystals share the primary crystals' orientation, it does not explain why. One possibility is that the amorphous phase is oriented during film blowing, thus directing the secondary crystals to form with a preferred orientation. However, the amorphous phase in such low-crystallinity blown films would not be expected to show significant orientation. Indeed, measurements by van Gurp et al. [37] on LDPE blown films reveal no amorphous phase orientation even when the crystalline phase is more oriented than in our blown films [22] of Zn46-12. An alternative possibility, which does not require amorphous phase orientation to be invoked, is that the lateral extent of the secondary crystals dictates their orientation. The average spacing d between

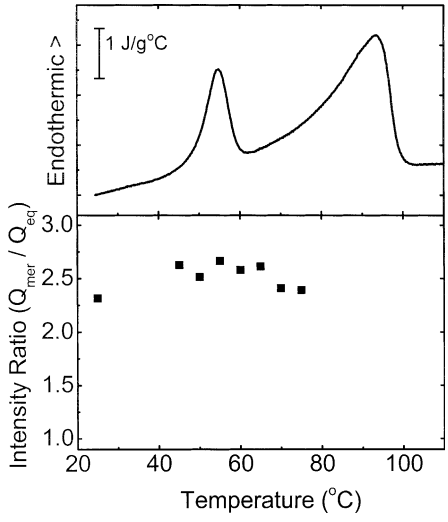

Fig. 7. Top panel: DSC heating thermogram of Zn46-12 at 10 °C/min. Bottom panel: relative SAXS invariant ratio Q_{mer}/Q_{eq} for the Zn46-12 blown film as a function of temperature, reflecting the anisotropy of the crystals.

primary crystals is approximately 12 nm, from the value of $2\pi/q^*$ along the meridian in Fig. 6 at 75 °C. Secondary crystals with lateral extents much smaller than this should be isotropic, as their orientation is essentially unconstrained by the framework of primary crystals. On the other hand, interlamellar secondary crystals with lateral extents near or above 12 nm can only be present if they follow the orientation of the primary crystals. Since, these secondary crystals are thin ($\approx$3 nm), they must thus have an aspect ratio ($\geq$4) more akin to that of a plate-like crystal than to an isotropic fringed micelle. Even if secondary crystals nucleate and grow with all possible orientations, only those with their normals generally aligned with those of the primary crystals can grow to a large lateral extent; consequently, these aligned secondary crystals will dominate the ensemble orientation probed by scattering, consistent with our observation.

4. Conclusions

The ubiquitous low-temperature endotherm in aged E/MAA ionomers reflects the melting of thin, interlamellar secondary crystals. Such small crystals contribute only modestly to the crystalline reflections observed by WAXD, but strongly alter the SAXS pattern by greatly decreasing the average intercrystallite separation. Though these materials are less than 50% crystalline, melting the secondary crystals causes an increase in the invariant, due to a substantial reduction in the electron density of the amorphous phase and a consequent increase in the crystal-amorphous electron density contrast. These secondary crystals are much thinner than the average amorphous layer between primary crystals, yet variable-temperature 2D SAXS on a highly-oriented film shows that the secondary and primary crystals have a common orientation. This indicates that, like the primary crystals, the secondary crystals have a substantial lateral extent.

Acknowledgements

Financial support for this work came from DuPont Packaging and Industrial Polymers and from the National Science Foundation, Polymers Program (DMR-9711436 and DMR-0220236). We thank Dr John W. Paul (DuPont) for providing Zn80-11 and the corresponding E/MAA copolymer; Dr David M. Dean (DuPont) for the blown film of Zn46-12; and Dr Stephanie T. Lopina (Princeton) for the neutralization of Na16-11. We are also grateful to Dr Fengji Yeh for his assistance with the synchrotron experiments, and to Professor Anthony J. Ryan for the use of his Linkam DSC600.

References

[1] Eisenberg A, Kim JS. Introduction to ionomers. New York: Wiley; 1998.
[2] Longworth R, Vaughan DJ. Nature 1968;218(5136):85–7.
[3] Register RA, Cooper SL. Macromolecules 1990;23(1):318–23.
[4] Marx CL, Cooper SL. J Macromol Sci Phys 1974;B9(1):19–33.
[5] Tsujita Y, Shibayama K, Takizawa A, Kinoshita T. J Appl Polym Sci 1987;33(4):1307–14.
[6] Huang YE. MSE Thesis, Princeton University; 2001.
[7] Kohzaki M, Tsujita Y, Takizawa A, Kinoshita T. J Appl Polym Sci 1987;33(7):2393–402.
[8] Schawe JEK. Thermochim Acta 1995;260:1–16.
[9] Androsch R, Wunderlich B. Macromolecules 1999;32(21):7238–47.
[10] Kuwabara K, Horii F. J Polym Sci Part B: Polym Phys 2002;40(11): 1142–53.
[11] Alizadeh A, Richardson L, Xu J, McCartney S, Marand H, Cheung YW, et al. Macromolecules 1999;32(19):6221–35.
[12] Tadano K, Hirasawa E, Yamamoto H, Yano S. Macromolecules 1989; 22(1):226–33.
[13] Ray AK. J Therm Anal 1996;46(6):1527–39.
[14] Akimoto H, Kanazawa T, Yamada M, Matsuda S, Shonaike GO, Murakami A. J Appl Polym Sci 2001;81(7):1712–20.
[15] Kutsumizu S, Goto M, Yano S. Macromolecules 2004;37(13):4821–9.
[16] Wilson FC, Longworth R, Vaughan DJ. ACS Polym Prepr 1968;9(1): 505–14.
[17] Jia Y, Kleinhammes A, Wu Y. Macromolecules 2005;38(7):2781–5.
[18] Longworth R. Thermoplastic ionic polymers: ionomers. In: Holliday L, editor. Ionic polymers. New York: Wiley; 1975. p. 69–172.
[19] Vanhoorne P, Register RA. Macromolecules 1996;29(2):598–604.
[20] Tierney NK, Register RA. Macromolecules 2002;35(6):2358–64.
[21] Annual Book of ASTM Standards. Philadelphia, PA: American Society for testing and materials; 1976. Part 35, p. 427–37.
[22] Lee LBW, Register RA, Dean DM. J Polym Sci Part B: Polym Phys 2005;43(1):97–106.
[23] Quiram DJ, Register RA, Marchand GR, Adamson DH. Macromolecules 1998;31(15):4891–8.
[24] Quiram DJ, Register RA, Ryan AJ. Macromolecules 1998;31(4): 1432–5.
[25] Russell TP. Small-angle scattering. In: Brown GS, Moncton DE, editors. Handbook on synchrotron radiation, vol. 3. Amsterdam: North-Holland; 1991. p. 379–469.
[26] Loo YL, Register RA, Hsiao BS. ACS PMSE Proc 1999;81:294–5.
[27] Wunderlich B. Macromolecular physics. Crystal melting. vol. 3. New York: Academic Press; 1980.
[28] Baltá-Calleja FJ, Vonk CG. X-ray scattering of synthetic polymers. Amsterdam: Elsevier; 1989 p. 270–94.
[29] Crist B. Macromolecules 2003;36(13):4880–90.
[30] Register RA. Unpublished.
[31] Crist B. Polymer 2003;44(16):4563–72.
[32] Farrell KV, Grady BP. Macromolecules 2000;33(19):7122–6.
[33] Porod G. General theory. In: Glatter O, Kratky O, editors. Small angle X-ray scattering. New York: Academic Press; 1982. p. 17–51.
[34] Pilz I. J Colloid Interface Sci 1969;30(1):140–4.
[35] Loo YL, Register RA. Unpublished.
[36] Flory PJ. Principles of polymer chemistry. Ithaca, NY: Cornell University Press; 1953.
[37] van Gurp M, Kip BJ, van Heel JPC, de Boer B. J Plast Film Sheet 1994;10:156–76.